Amyloid-β and tau synergistically impair the oxidative phosphorylation system in triple transgenic Alzheimer's disease mice

Virginie Rhein[a], Xiaomin Song[b], Andreas Wiesner[c], Lars M. Ittner[c], Ginette Baysang[a], Fides Meier[a], Laurence Ozmen[d], Horst Bluethmann[d], Stefan Dröse[e], Ulrich Brandt[e], Egemen Savaskan[a,f], Christian Czech[d], Jürgen Götz[c,g], and Anne Eckert[a,1]

[a]Neurobiology Laboratory for Brain Aging and Mental Health, Psychiatric University Clinics, University of Basel, 4025 Basel, Switzerland; [b]Australian Proteome Analysis Facility, Macquarie University, Sydney NSW 2109, Australia; [c]Alzheimer's and Parkinson's Disease Laboratory, Brain and Mind Research Institute, University of Sydney, 100 Mallett Street, Camperdown NSW 2050, Australia; [d]Hoffmann-La-Roche AG, Pharma Research, Neurosciences, 4070 Basel, Switzerland; [e]Molecular Bioenergetics Group, Medical School, Cluster of Excellence Frankfurt Macromolecular Complexes, Center for Membrane Proteomics, Johann Wolfgang Goethe-Universität, 60590 Frankfurt am Main, Germany; [f]Division of Psychiatric Research and Hospital for Psychogeriatric Medicine, University of Zurich, 8032 Zurich, Switzerland; and [g]The Medical Foundation, University of Sydney, Camperdown NSW 2050, Australia

Edited by L. L. Iversen, University of Oxford, Oxford, United Kingdom, and approved September 29, 2009 (received for review July 2, 2009)

Alzheimer's disease (AD) is characterized by amyloid-beta (Aβ)-containing plaques, neurofibrillary tangles, and neuron and synapse loss. Tangle formation has been reproduced in P301L tau transgenic pR5 mice, whereas APP^{sw}PS2^{N141I} double-transgenic APP152 mice develop Aβ plaques. Cross-breeding generates triple transgenic (^{triple}AD) mice that combine both pathologies in one model. To determine functional consequences of the combined Aβ and tau pathologies, we performed a proteomic analysis followed by functional validation. Specifically, we obtained vesicular preparations from ^{triple}AD mice, the parental strains, and nontransgenic mice, followed by the quantitative mass-tag labeling proteomic technique iTRAQ and mass spectrometry. Within 1,275 quantified proteins, we found a massive deregulation of 24 proteins, of which one-third were mitochondrial proteins mainly related to complexes I and IV of the oxidative phosphorylation system (OXPHOS). Notably, deregulation of complex I was tau dependent, whereas deregulation of complex IV was Aβ dependent, both at the protein and activity levels. Synergistic effects of Aβ and tau were evident in 8-month-old ^{triple}AD mice as only they showed a reduction of the mitochondrial membrane potential at this early age. At the age of 12 months, the strongest defects on OXPHOS, synthesis of ATP, and reactive oxygen species were exhibited in the ^{triple}AD mice, again emphasizing synergistic, age-associated effects of Aβ and tau in perishing mitochondria. Our study establishes a molecular link between Aβ and tau protein in AD pathology in vivo, illustrating the potential of quantitative proteomics.

amyloid-beta peptide | electron transport chain | energy metabolism | mitochondrial complexes | tau protein

Alzheimer's disease (AD) is a devastating neurodegenerative disorder affecting >15 million people worldwide (1). The key histopathological features are amyloid-beta (Aβ)-containing plaques and microtubule-associated protein tau-containing neurofibrillary tangles (NFTs), along with neuronal and synapse loss in selected brain areas (2, 3). In determining the role of distinct proteins in these processes, traditionally, candidate-driven approaches have been pursued, linking neuronal dysfunction to the distribution of known proteins in healthy compared with degenerating neurons, or in transgenic compared with control brain. In comparison, proteomics offers a powerful nonbiased approach as shown by us previously (4, 5).

APP152 (APP/PS2) double-transgenic mice model the Aβ plaque pathology of AD (6); they coexpress the N141I mutant form of PS2 together with the APP^{sw} mutant found in familial cases of AD. The mice display age-related cognitive deficits associated with discrete brain Aβ deposition and inflammation (6). pR5 mice model the tangle pathology of AD (7–9). They express P301L mutant tau found in familial cases of frontotemporal dementia (FTD), a dementia related to AD. The pR5 mice show a hippocampus- and amygdala-dependent behavioral impairment related to AD (10). Crossing of pR5 and APP/PS2 mice revealed that total tau and APP levels, respectively, were not altered in ^{triple}AD mice, suggesting that there is no titration of transcription factors for the promoters driving either mutant APP or tau transgene expression (11). Of particular relevance in the ^{triple}AD mice is the low interanimal variability and early onset of tau pathology (11).

Here, we performed a comparative, quantitative proteomic analysis of single-transgenic pR5, double-transgenic APP/PS2, and ^{triple}AD (pR5/APP/PS2) mice, as well as wild-type controls, and found that one-third of the deregulated proteins were mitochondrial. In evaluating our findings, we could establish mitochondrial dysfunction in ^{triple}AD mice, synergistically induced by tau and Aβ pathologies.

Results

Comparative iTRAQ (Isobaric Tags for Relative and Absolute Quantitation) Mass Spectrometry. Crude vesicular fractions of forebrains obtained from 10-month-old single-transgenic pR5 mice, double-transgenic APP/PS2 mice, a cross of the 2 strains (^{triple}AD), and nontransgenic littermate controls were trypsin digested (n = 6 animals for each group), and peptides labeled with iTRAQ. Then, these were separated by HPLC, using both reverse-phase (RP) and strong cation exchange (SCX) columns, followed by nanoLC-ESI MS/MS mass spectrometry (3 iTRAQ runs and 4 two-dimensional LC ESI MS/MS data sets were used to obtain iTRAQ data). Data processing identified 1,598 proteins, 1,539 of which were quantified; 1,275 with more than 2 peptides. Twenty-four proteins were found to be differentially expressed in ^{triple}AD compared with the other samples (Table 1 and Table S1).

Deregulated Proteins Identified by iTRAQ. ProteinPilot requires a minimum of 40 counts of iTRAQ reporting ion intensities to

Author contributions: A.E. designed research; V.R., X.S., A.W., L.M.I., G.B., F.M., S.D., U.B., E.S., and J.G. performed research; L.O., H.B., and C.C. contributed new reagents/analytic tools; V.R. and X.S. analyzed data; and J.G. and A.E. wrote the paper.

The authors declare no conflict of interest.

This article is a PNAS Direct Submission.

Freely available online through the PNAS open access option.

[1]To whom correspondence should be addressed at: Neurobiology Laboratory for Brain Aging and Mental Health, Associated Research Group, Department of Biomedicine, Psychiatric University Clinics, University of Basel, Wilhelm Klein-Strasse 27, CH-4025 Basel, Switzerland. E-mail: anne.eckert@upkbs.ch.

This article contains supporting information online at www.pnas.org/cgi/content/full/0905529106/DCSupplemental.

NEUROSCIENCE

Table 1. iTRAQ ratios (wild-type vs. ^{triple}AD, pR5 vs. ^{triple}AD, and APP/PS2 vs. ^{triple}AD) showing differentially expressed proteins observed by iTRAQ experiment

Accession no.	Name	Wild-type vs. ^{triple}AD	pR5 vs. ^{triple}AD	APP/PS2 vs. ^{triple}AD
ANXA5_MOUSE (P48036)	Annexin A5 (Annexin V) (Lipocortin V)	1.28		0.63
ANXA6_MOUSE (P14824)	Annexin A6 (Annexin VI) (Lipocortin VI)	1.46	2.2	
ARF3_MOUSE (P61205)	ADP-ribosylation factor 3			0.65
BASP_MOUSE (Q91XV3)	Brain acid soluble protein 1 (BASP1 protein)		1.51	
CALM_MOUSE (P62204)	Calmodulin (CaM)		0.78	0.65
COX2_MOUSE (P00405)	**Cytochrome c oxidase subunit 2 (EC 1.9.3.1)**	**1.22**	**1.42**	
COX41_MOUSE (P19783)	**Cytochrome c oxidase subunit IV isoform 1, mitochondrial precursor (EC 1.9.3.1)**	**1.36**	**1.47**	
COX5A_MOUSE (P12787)	**Cytochrome c oxidase polypeptide Va, mitochondrial precursor (EC 1.9.3.1)**	**1.21**	**1.43**	
COX5B_MOUSE (P19536)	**Cytochrome c oxidase polypeptide Vb, mitochondrial precursor (EC 1.9.3.1)**		**1.33**	
CX7A2_MOUSE (P48771)	**Cytochrome c oxidase polypeptide VIIa-liver/heart, mitochondrial precursor (EC 1.9.3.1)**	**1.41**	**1.69**	
HBA_MOUSE (P01942)	Hemoglobin alpha subunit	0.73	0.69	
HBB1_MOUSE (P02088)	Hemoglobin beta-1 subunit chain	0.69		0.6
MBP_MOUSE (P04370)	Myelin basic protein (MBP) (Myelin A1 protein)	1.32		1.22
NDKA_MOUSE (P15532)	Nucleoside diphosphate kinase A (EC 2.7.4.6)			0.56
NIDM_MOUSE (Q9DCS9)	**NADH-ubiquinone oxidoreductase PDSW subunit (EC 1.6.5.3)**		**1.39**	**0.66**
NUCM_MOUSE (Q91WD5)	**NADH-ubiquinone oxidoreductase 49 kDa subunit, mitochondrial precursor (EC 1.6.5.3)**			**0.8**
NUIM_MOUSE (Q8K3J1)	**NADH-ubiquinone oxidoreductase 23 kDa subunit, mitochondrial precursor (EC 1.6.5.3)**	**1.22**		
PHB_MOUSE (P67778)	Prohibitin (B-cell receptor associated protein 32) (BAP 32)			0.77
PPIA_MOUSE (P17742)	Peptidyl-prolyl cis-trans isomerase A (EC 5.2.1.8)			1.4
S12A2_MOUSE (P55012)	Solute carrier family 12 member 2 symporter)		1.49	
SYN2_MOUSE (Q64332)	Synapsin-2 (Synapsin II)		1.69	
TAU_MOUSE (P10637)	Microtubule-associated protein tau (Neurofibrillary tangle protein)	0.64		0.6
THY1_MOUSE (P01831)	Thy-1 membrane glycoprotein precursor	1.4	1.94	
VA0D_MOUSE (P51863)	Vacuolar ATP synthase subunit d	1.35	1.71	0.77

Wild-type and ^{triple}AD mouse samples are compared to other types. Only iTRAQ ratios satisfying the criterion (P value < 0.01 and $0.82 <$ iTRAQ ratio < 1.2) with the same ratio-changing trends in a minimum of 2 of the 3 independent iTRAQ runs and not having ratio-changing trends in any other runs are listed. Deregulated subunits of complexes I and IV are bold.

calculate iTRAQ ratios. Proteins identified with iTRAQ tag ion intensities below this threshold were not quantified. In our study, ≈90% of the identified proteins had iTRAQ ratios (Fig. S1*A*), and of these, ≈80% were calculated from more than 2 peptides.

We tabulated iTRAQ ratios of all proteins using the ^{triple}AD as denominator and iTRAQ ratios >1.2 or <0.82 with a P value <0.01 as threshold to identify deregulated proteins as listed in Table 1. A protein had to show the same deregulation trend in at least 2 of the 3 runs to be considered as deregulated. From our past experience iTRAQ ratios >1.2 or <0.82 with a P value <0.01 indicate protein differences of at least 1.5-fold.

Consistent with transgenic tau expression, the experimental data show that tau is significantly up-regulated in pR5 mice and ^{triple}AD mouse brain compared with wild-type and APP/PS2 mice. We performed an overrepresentation analysis using the Gene Ontology (GO) database to perform a functional characterization of the deregulated proteins and established a GO map as described in ref. 12. This revealed that one-third of the proteins have functions in mitochondria, specifically complex I and IV (Table 1). In agreement, separation of mitochondrial complexes from cortical brain by 2D resolution confirmed a similar deregulation of the 49-kDa subunit of complex I and subunits II and IV of complex IV (Fig. S1 *B* and *C*). Therefore, we decided to assess ^{triple}AD compared with pR5 and APP/PS2 mice for mitochondrial function.

^{Triple}AD Mice Exhibit Strong Defects in Mitochondrial OXPHOS, Complex Activities, and Energy Homeostasis. A high-resolution respiratory system has been used to evaluate the capacity of the entire oxidative phosphorylation system (OXPHOS) of cerebral mitochondria from the 4 mouse strains (Fig. 1*A*). We determined flux control ratios to obtain information on metabolic states of respiration. The respiratory control ratio (RCR3/4) is an indicator of the state of coupling of mitochondria. State 3 is the rate of phosphorylating respiration in the presence of exogenous ADP, and state 4 is associated with proton leakage across the inner mitochondrial membrane in the absence of ADP. Our findings suggest a pronounced decrease of RCR3/4 in mitochondria from APP/PS2 and ^{triple}AD compared with age-matched wild-type mice (Fig. 1*B*). When we examined the ETS/ROX (electron transport system/residual oxygen consumption) ratio, which yields an index of the maximum oxygen consumption capacity relative to the magnitude of residual oxygen consumption, we found that it was also decreased in APP/PS2 and ^{triple}AD compared with age-matched wild-type mice (Fig. 1*C*). We have shown previously that respiration of mitochondria from pR5 mice is reduced compared with wild-type controls, but not until the age of 24 months (4) (Fig. S2). In contrast, APP/PS2 mitochondria showed a decrease in OXPHOS compared with wild-type already at the age of 8 months (Fig. 1*D*). At this age, OXPHOS of brain mitochondria from ^{triple}AD mice did not differ compared with that of age-matched APP/PS2 mitochondria (Fig. 1*E*), but it was significantly decreased in ^{triple}AD mice at the age of 12 months (Fig. 1 *F* and *G*). Taken together, with increasing age, the global failure of the mitochondrial respiratory capacity deteriorated the strongest in mitochondria from

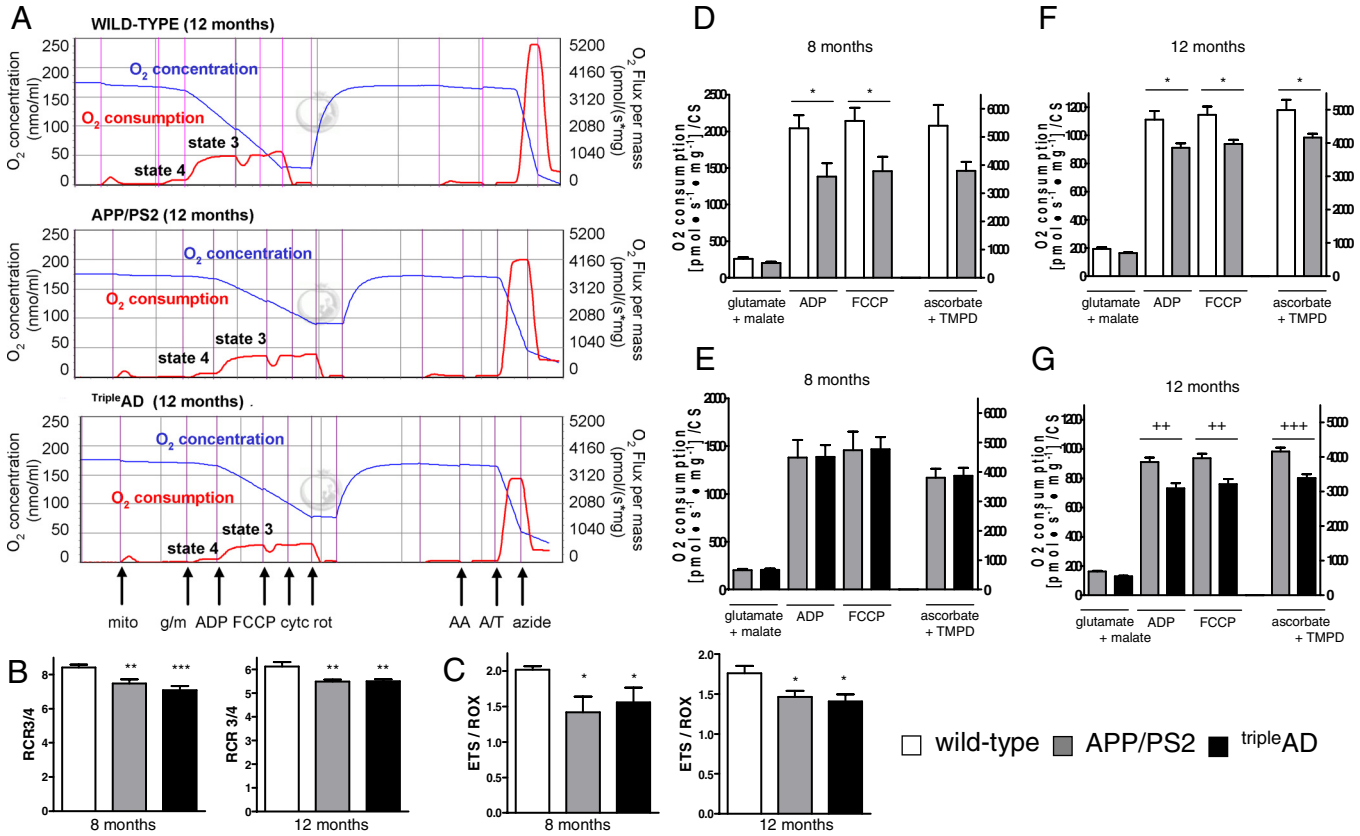

Fig. 1. High-resolution respiratory system reveals a heightened defect in the mitochondrial OXPHOS from brains of ^{triple}AD mice. Measurement of oxygen (O_2) flux and consumption in freshly isolated mitochondria from cortical brains of age-matched wild-type, APP/PS2, and ^{triple}AD mice. After detection of endogenous respiration (mito), glutamate+malate (g/m) were added to induce state 4 respiration. ADP stimulated state 3 respiration. After determining coupled respiration, FCCP was added and the maximal respiratory capacity measured in the absence of a proton gradient. Cytochrome c (cyt c) demonstrated mitochondrial membrane integrity. To inhibit activities of complexes I–III, rotenone (rot) and antimycine A (AA) were added. Complex IV activity was stimulated by ascorbate/TMPD (A/T) before terminating mitochondrial respiration by adding sodium azide (azide). O_2 consumption was normalized to the corresponding citrate synthase (CS) activity. (*A*) Representative diagrams of O_2 flux and consumption in mitochondria from 12-month-old wild-type, APP/PS2, and ^{triple}AD mice in response to titrated substrates and inhibitors of mitochondrial complexes. (*B*) RCR3/4 (state3/state4 ratio) representing the mitochondrial coupling state was reduced in 8- and 12-month-old APP/PS2 and ^{triple}AD mice. (*C*) ETS/ROX ratio, which yields an index of the maximum oxygen consumption capacity of the electron transport system (ETS) relative to the magnitude of residual oxygen consumption (ROX), was reduced in 8- and 12-month-old APP/PS2 and ^{triple}AD mice compared with age-matched wild-type mitochondria. (*D*) Two-way ANOVA revealed a significant effect of the transgene on the respiratory rates of mitochondria between 8-month-old wild-type and APP/PS2 mice ($P < 0.001$). (*E*) No difference was observed in respiration between 8-month-old APP/PS2 and ^{triple}AD mice. (*F*) At 12 months of age, respiration differed again significantly between wild-type and APP/PS2 ($P < 0.001$) and (*G*) between APP/PS2 and ^{triple}AD mice ($P < 0.001$). (*B* and *C*) One-way ANOVA post hoc Tukey's. (*D*–*G*) Two-way ANOVA post hoc Bonferroni. *, $P < 0.05$; **, $P < 0.01$; ***, $P < 0.001$ vs. wild-type; $^{++}$, $P < 0.01$; $^{+++}$, $P < 0.001$ vs. APP/PS2 (n = 7–12 animals/group).

^{triple}AD mice, suggesting a synergistic destructive effect of tau and Aβ on mitochondria.

Next, we used a direct measurement of the specific activity of complex I in freshly isolated brain mitochondria, i.e., NADH-ubiquinone oxidoreductase activity measured as NADH:DBQ activity that was then normalized to complex I content (NADH:HAR activity). At 8 months, complex I activity was only decreased in pR5 mice, confirming our previous data about complex I deficiency in these mice (4) (Fig. 2*A*). At 12 months of age, all 3 transgenic mouse models exhibited a significant decrease of DBQ/HAR compared with wild-type mice (Fig. 2*A*). Interestingly, at the age of 12 months, content of complex I (measured by HAR activity) was increased in ^{triple}AD mice, suggesting a compensatory up-regulation in response to functional deficits of this complex (Fig. S3). Similarly, compared with APP/PS2 mice, complex I proteins were found to be up-regulated (Table 1). Activity of citrate synthase (CS), a pace-making enzyme in the first step of the Krebs cycle, thought to be proportional to the content of OXPHOS enzymes (13), was increased in 8-month-old APP/PS2 and ^{triple}AD mice. At 12 months, the increase persisted only in cortical mitochondria from ^{triple}AD mice, suggesting a compensatory incapacity to restore a physiological state specifically in this mouse model that exhibits the strongest AD pathology of both plaques and tangles (Fig. 2*B*).

At the age of 8 months, APP/PS2 and ^{triple}AD mice showed a significantly decreased complex IV activity (CIV/CS ratio) (Fig. 2*C*). This decrease became more marked at the age of 12 months, when the accumulation of defects in the single complexes as well as in the entire OXPHOS, respectively, could not be further compensated as shown by a drop in ATP levels in cortical brain cells from APP/PS2 and ^{triple}AD mice, with the strongest decrease seen in the latter (Fig. 2*D*). This indicates a general disturbance of cellular energy homeostasis in the cortices of these mice. The effect was brain region-specific as no difference in ATP levels was observed in cerebellar cells from the same mice (Fig. S4).

Aβ and Hyperphosphorylated Tau Cause a Decreased Mitochondrial Membrane Potential (MMP). Based on our recent in vitro results that cortical brain cells from pR5 mice are particularly sensitive to synthetic Aβ insult (14, 15), we determined the mitochondrial

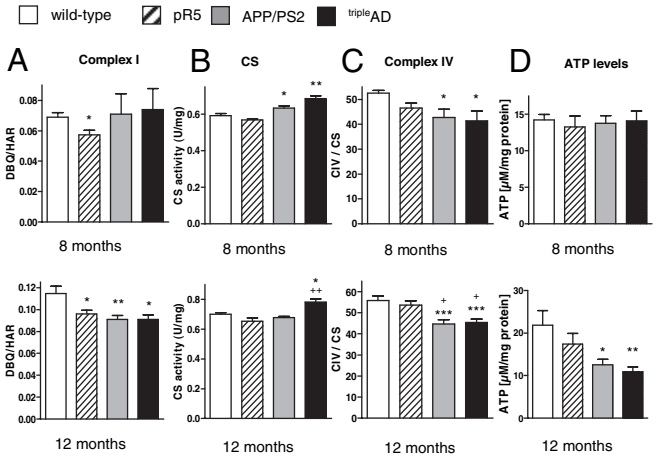

Fig. 2. Impaired mitochondrial enzyme activities and decreased ATP levels in cortical brain cells from tripleAD mice. (*A*) Complex I activity (DBQ/HAR ratio) was decreased in 8-month-old pR5 mitochondria. At 12 months, all 3 transgenic mouse models presented a decrease in complex I activity. (*B*) Citrate synthase (CS) activity was increased in 8-month-old APP/PS2 and tripleAD mice. At 12 months, the increase persisted only in tripleAD mice. (*C*) Complex IV activity (CIV/CS ratio) was decreased in APP/PS2 and tripleAD mitochondria at 8 months of age. The decrease became more pronounced at the age of 12 months. (*D*) ATP levels were reduced in 12-month-old APP/PS2 and triple mice. (*A–D*) One-way ANOVA post hoc Tukey's. *, $P < 0.05$; **, $P < 0.01$; ***, $P < 0.001$ vs. wild type; $^{+}$, $P < 0.05$ vs. pR5 (n = 7–12 animals/group).

membrane potential (MMP) that is widely considered as an indicator of mitochondrial functionality (16). Basal MMP was significantly and exclusively reduced in cortical cells from 8-month-old tripleAD mice. At 12 months, MMP was additionally reduced in cortical cells from APP/PS2 mice (Fig. 3*A*). Importantly, the same results were obtained using a different fluorescent dye (R123; Fig. S5). Again, this effect was brain region-specific as it was not observed for the cerebellum (Fig. S6).

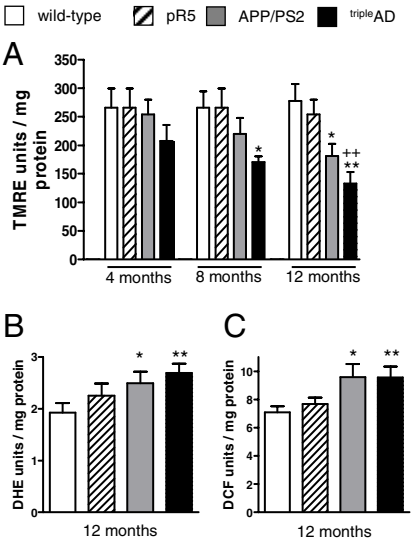

Fig. 3. Reduced MMP and increased ROS levels in cortical brain cells from tripleAD mice. (*A*) MMP (TMRE fluorescence units/mg protein) was reduced in cortical cells from 8-month-old tripleAD mice. At the age of 12 months, MMP was also reduced in cells from APP/PS2 mice. (*B*) Levels of superoxide anion radicals (DHE fluorescence units/mg protein) and (*C*) cytosolic ROS (DCF fluorescence units/mg protein) were increased in cells from 12-month-old APP/PS2 and tripleAD mice. (*A–C*) One-way ANOVA post hoc Tukey's. *, $P < 0.05$; **, $P < 0.01$; vs. wild-type, $^{++}$, $P < 0.01$ vs. pR5 (n = 7–12 animals/group).

Increased Mitochondrial Failure Is Accompanied by Enhanced Reactive Oxygen Species (ROS) Production. Superoxide anion levels were enhanced in cortical brain cells of 12-month-old APP/PS2 mice and markedly increased in those of age-matched tripleAD mice (Fig. 3*B*). In addition, cytosolic ROS levels were enhanced in brain cells from APP/PS2 and tripleAD mice (Fig. 3*C*). These differences were only observed at an age of 12, and not 8 months (Fig. S7 *A* and *B*), suggesting that at the older age, brain mitochondria are not capable of compensating their respiratory failure.

Discussion

Energy deficiency and mitochondrial dysfunction have been recognized as a prominent, early event in AD, but the mechanisms leading to mitochondrial failure are not well understood (15, 17–24). Recently, we had shown in vivo that P301L mutant tau was capable of inducing mitochondrial dysfunction and increasing levels of ROS in pR5 mice (4). We had also found an increased mitochondrial vulnerability of pR5 cortical brain cells toward Aβ in vitro (4, 14). However, the relative contribution of tau and Aβ remained unclear, as did possible synergistic effects. To address this, we investigated brains of pR5, APP/PS2, and tripleAD (pR5/APP/PS2) mice, the latter combining Aβ and tau pathologies.

In the present study we could clearly show that with increasing age, both Aβ and tau synergistically impair mitochondrial function and energy homeostasis in vivo. At 8 months of age, in agreement with previous data (4), complex I activity was only decreased in pR5, and not in APP/PS2 and tripleAD mice, indicating a tau-specific sensitivity of complex I of OXPHOS. In contrast, activity of CS, a pace-making enzyme of the Krebs cycle, was increased in 8-month-old APP/PS2 and tripleAD mice. At this age, a robust cortical pathology of Aβ plaques and tau deposits is present (11). Because CS activity seems to be proportional to the content of enzymes of OXPHOS (13), the increased activity can be interpreted as compensatory mechanism of mitochondria in response to OXPHOS failure, a mechanism initiated in tripleAD mice already at the age of 4 months, when Aβ accumulation and abnormal tau phosphorylation (such as of epitope T231) become evident (11). Notably, at this early age, cortical brain cells from tripleAD mice exhibit already a tendency to reduced MMP, suggesting that this is a very sensitive indicator of early mitochondrial failure. The decrease in MMP (that was not seen in the parental strains) further continued until tripleAD mice reached 8 months of age, emphasizing a synergistic action of Aβ and tau. At 12 months, increased Aβ levels per se were able to reduce MMP, because a significant reduction was present also in APP/PS2 mice, but the reduction of MMP was more pronounced in tripleAD mice.

Complex IV activity was decreased in APP/PS2 and tripleAD cortices at 8 months of age, but not in pR5, confirming related findings that it is mainly the Aβ pathology that affects complex IV activity, both in vivo and in vitro (22, 25). In APP/PS2 compared with wild-type mice, an impairment of OXPHOS as detected by decreased oxygen consumption was seen at this age, suggesting an earlier and stronger effect of the Aβ/APP pathway on this vulnerable mitochondrial system compared with tau, as oxygen consumption of pR5 mitochondria was reduced, but not until the mice reached 24 months of age (4). Similarly, both flux control ratios RCR3/4 and ETS/ROX, which measure metabolic states of mitochondrial respiration, were similarly decreased in APP/PS2 and tripleAD mitochondria, indicating an Aβ-induced increase of the uncoupling state of these organelles. The data indicate that Aβ affects mitochondrial function more extensively and at different levels of respiration and function than tau does, which only shows an early effect on the activity of a single complex of OXPHOS, but evidently increases the vulnerability to Aβ toxicity in vivo. Notably, at 8 months, no change in cellular

energy homeostasis or oxidative stress levels was evident, suggesting an efficient compensatory machinery within brain cells at this age.

However, as the mice aged, impairment of OXPHOS and mitochondrial enzyme activities was aggravated, especially in the presence of both plaques and tangles. Indeed, despite compensatory mechanisms—increased complex I content and CS activity—the defects of complex I and IV became more marked at 12 months, indicating a failure to restore the bioenergetic homeostasis in ^{triple}AD mice as they age. Then, we also observed a difference in oxygen consumption between APP/PS2 and ^{triple}AD mice as well as a drop in ATP levels, with the strongest decrease found in ^{triple}AD, again suggesting a synergistic action of the 2 lesions on mitochondria. These mitochondrial defects were associated with an increase of superoxide anion, as well as cytosolic ROS levels in 12-month-old APP/PS2, and were most pronounced in ^{triple}AD mice, suggesting that at this older age detoxifying mechanisms fail to balance increased ROS production, which in turn might further damage mitochondrial OXPHOS.

In agreement with our functional data, iTRAQ MS identified 3 deregulated subunits of complex I in ^{triple}AD mice: NUCM, NUIM, and NIDM. NUCM likely has a central role within the catalytic core of mitochondrial complex I (26). Interestingly, NUCM and NIDM were up-regulated in ^{triple}AD brain, probably as a compensatory response to the functional failure of OXPHOS. These data nicely correspond with the detected increase in complex I content (detected by HAR activity). Inversely, NUIM, which is thought to participate in the electron transfer and proton-pumping activities of complex I, is down-regulated in ^{triple}AD mice. Together, these findings emphasize that Aβ and tau synergistically impair complex I function with aging. On the contrary, changes in the expression of complex IV subunits seem to be mainly related to Aβ. Indeed, a down-regulation of several subunits of complex IV is essentially seen between pR5 and ^{triple}AD mice, but not between APP/PS2 and ^{triple}AD mice. Furthermore, our findings of a mitochondrial dysfunction in ^{triple}AD mice are supported by a significant deregulation of mitochondria-related proteins: calmodulin, a small, ubiquitous Ca^{2+}-binding protein, and its putative target, the transmembrane proteolipid pore of the vacuolar or vesicular ATPase (V-ATPase V0) sector subunit a1, with calmodulin functioning in an ATPase V (0)-dependent manner at synapses (27). Interestingly, both proteins are deregulated in ^{triple}AD mice. Deregulation of proteins with expression in glial cells, e.g., myelin basic protein, may indicate additional damage of nonneuronal cells. However, because expression of Aβ and tau in our mouse models is neuron-specific, mitochondria from neurons likely represent the primary toxic target, but with disease progressing, cells in the vicinity are likely to be also impacted and damaged.

Our findings are in line with recent studies associating Aβ and tau with oxidative stress (17, 18, 28). Moreover, APP transport was shown to be impaired by elevated tau, suggesting a possible link of the 2 proteins (28, 29). Oligomeric Aβ can attach to tau (30, 31), causing a rapid dissociation of tau from microtubules and a collapse of axonal structures leading initially to synaptic malfunction and ultimately, neuronal death. Interestingly, Aβ may not only be located to the cell surface but also directly interact with mitochondria (20) as it can be imported into mitochondria via the translocase of the outer membrane (TOM) machinery (32). A crucial role for mitochondria in AD is further underpinned by findings linking maternal inheritance of mitochondrial DNA to both predisposition of AD and glucose hypometabolism (33) that may reflect energy disturbances as found, e.g., in our ^{triple}AD model.

Together, our studies highlight the key role of mitochondria in AD pathogenesis, and the close interrelationship of this organelle and the two main pathological features of the disease. This was obtained by combinatorial transgenesis, quantitative proteomics, and functional assays. We show that disturbances in the respiratory and energy system of ^{triple}AD mice are due to (*i*) a convergence of Aβ and tau on mitochondria, accelerating defects in respiratory capacity, and (*ii*) a main defect in mitochondrial complexes I and IV. Moreover, we found (*iii*) that age-related oxidative stress may exaggerate the dysfunctional energy metabolism in a vicious cycle, finally leading to cell death. Our data complement those obtained in a second ^{triple}TG mouse model (34). They may contribute to a better understanding of these biochemical pathways and assist in the development of antioxidative treatments. Importantly, we could reveal defects of mitochondrial respiratory capacity and a failure to restore energy homeostasis in mice with plaques and tangles in vivo, consolidating the idea that a synergistic effect of tau and Aβ augments the pathological deterioration of mitochondria.

Materials and Methods

Mice Used for the Studies. Four strains of mice were investigated: single-transgenic pR5 (7), double-transgenic APP/PS2 (6), a crossbreeding (^{triple}AD) (11), and nontransgenic wild-type littermate controls. For the proteomic analysis, 6 female mice were killed from each strain at 10 months of age, and forebrains dissected. For the functional studies, 7–12 female mice were killed from each strain at the age of 2, 4, 8, 12, and 16 months to identify the age when functional changes start, and forebrains dissected (see *SI Methods* and Table S2 for details).

Proteomic Approach. Crude synaptosomal preparations of forebrains from freshly killed mice were obtained for proteomic studies. The proteins were labeled using the iTRAQ technique and separated by both reverse-phase and strong cation exchange HPLC. Data were acquired by NanoLC-ESI MS/MS mass spectrometry and submitted to ProteinPilot for processing (see *SI Methods* for all details).

Cellular Analysis. Brain cells were obtained to determine mitochondrial function. The membrane potential of the inner mitochondrial membrane was measured using the dye tetramethylrhodamine ethyl ester (TMRE) and the dye rhodamine 123 (R123) (4). ATP content was determined using a bioluminescence assay (ViaLighTM HT; Cambrex Bio Science) (14). The total amount of mitochondria was measured using the cell-permeable mitochondria-selective dye. Finally, levels of ROS were measured using the fluorescent probe H2DCF-DA, and levels of superoxide anion radical using DHE (see *SI Methods* for all details).

Studies of Isolated Mitochondria. Mitochondria were isolated from mouse forebrains to investigate mitochondrial OXPHOS and respiratory capacity. Mitochondrial oxygen consumption was measured at 37 °C using an Oroboros Oxygraph-2k system (4, 21). Several mitochondrial enzyme activities (complex I, complex IV, and citrate synthase) were examined (13, 21) (see *SI Methods* for details).

Statistical Analysis. For statistical comparison in functional studies, Student's *t* test, one-way ANOVA followed by Tukey's post hoc test, and 2-way ANOVA followed by Bonferroni post hoc tests only for the oxygen consumption protocol, were used. Only P values <0.05 were considered as statistically significant. Data are represented as means ± SEM.

For iTRAQ statistics, P values were calculated for each protein ratio reported in the Pro Group™ Algorithm Results using ProteinPilot™ Software (Applied Biosystems). To be considered as significantly deregulated, iTRAQ ratios had to satisfy the criterion P value <0.01 and $0.82 <$ iTRAQ ratio < 1.2 (see *SI Methods* for all details).

ACKNOWLEDGMENTS. We thank Chris Clarke for strong cation exchange and reverse-phase fractionation. This research was supported by the Swiss National Science Foundation Grant SNF 310000–108223 (to A.E.), the University of Sydney, the Medical Foundation (University of Sydney), the National Health and Medical Research Council, the Judith Jane Mason and Harold Stannett Williams Memorial Foundation, the ARC, and by the New South Wales Government through the Ministry for Science and Medical Research (BioFirst Grant) (to J.G.), and Deutsche Forschungsgemeinschaft Grant SFB 815 (to U.B. and S.D.). The iTRAQ experiment was facilitated by access to Australian Proteome Analysis Facility which is funded by an initiative of the Australian Government as part of the National Collaborative Research Infrastructure Strategy.

1. Gotz J, *et al.* (2004) Transgenic animal models of Alzheimer's disease and related disorders: Histopathology, behavior and therapy. *Mol Psychiatry* 9:664–683.
2. Lee VM, Goedert M, Trojanowski JQ (2001) Neurodegenerative tauopathies. *Annu Rev Neurosci* 24:1121–1159.
3. Gotz J, Ittner LM (2008) Animal models of Alzheimer's disease and frontotemporal dementia. *Nat Rev Neurosci* 9:532–544.
4. David DC, *et al.* (2005) Proteomic and functional analyses reveal a mitochondrial dysfunction in P301L tau transgenic mice. *J Biol Chem* 280:23802–23814. Epub 2005 Apr 14.
5. David DC, *et al.* (2006) Beta-amyloid treatment of two complementary P301L tau-expressing Alzheimer's disease models reveals similar deregulated cellular processes. *Proteomics* 6:6566–6577.
6. Richards JG, *et al.* (2003) PS2APP transgenic mice, coexpressing hPS2mut and hAPPswe, show age-related cognitive deficits associated with discrete brain amyloid deposition and inflammation. *J Neurosci* 23:8989–9003.
7. Gotz J, Chen F, Barmettler R, Nitsch RM (2001) Tau filament formation in transgenic mice expressing P301L tau. *J Biol Chem* 276:529–534.
8. Gotz J, Chen F, van Dorpe J, Nitsch RM (2001) Formation of neurofibrillary tangles in P301l tau transgenic mice induced by Abeta 42 fibrils. *Science* 293:1491–1495.
9. Deters N, Ittner LM, Gotz J (2008) Divergent phosphorylation pattern of tau in P301L tau transgenic mice. *Eur J Neurosci* 28:137–147.
10. Pennanen L, Wolfer DP, Nitsch RM, Gotz J (2006) Impaired spatial reference memory and increased exploratory behavior in P301L tau transgenic mice. *Genes Brain Behav* 5:369–379.
11. Grueninger F, *et al.* (2009) Phosphorylation of Tau at S422 is enhanced by Abeta in TauPS2APP triple transgenic mice. *Neurobiol Dis*, in press.
12. Sugino K, *et al.* (2006) Molecular taxonomy of major neuronal classes in the adult mouse forebrain. *Nat Neurosci* 9:99–107.
13. Aleardi AM, *et al.* (2005) Gradual alteration of mitochondrial structure and function by beta-amyloids: Importance of membrane viscosity changes, energy deprivation, reactive oxygen species production, and cytochrome c release. *J Bionenerg Biomembr* 37:207–225.
14. Eckert A, *et al.* (2008) Oligomeric and fibrillar species of beta-amyloid (A beta 42) both impair mitochondrial function in P301L tau transgenic mice. *J Mol Med* 86:1255–1267.
15. Eckert A, *et al.* (2008) Soluble beta-amyloid leads to mitochondrial defects in amyloid precursor protein and tau transgenic mice. *Neurodegener Dis* 5:157–159.
16. Sompol P, *et al.* (2008) A neuronal model of Alzheimer's disease: An insight into the mechanisms of oxidative stress-mediated mitochondrial injury. *Neuroscience* 153:120–130.
17. Moreira PI, *et al.* (2008) Alzheimer disease and the role of free radicals in the pathogenesis of the disease. *CNS Neurol Disord Drug Targets* 7:3–10.
18. Su B, *et al.* (2008) Oxidative stress signaling in Alzheimer's disease. *Curr Alzheimer Res* 5:525–532.
19. Wang X, *et al.* (2008) Amyloid-beta overproduction causes abnormal mitochondrial dynamics via differential modulation of mitochondrial fission/fusion proteins. *Proc Natl Acad Sci USA* 105:19318–19323.
20. Lustbader JW, *et al.* (2004) ABAD directly links Abeta to mitochondrial toxicity in Alzheimer's disease. *Science* 304:448–452.
21. Rhein V, *et al.* (2009) Amyloid-beta leads to impaired cellular respiration, energy production and mitochondrial electron chain complex activities in human neuroblastoma cells. *Cell Mol Neurobiol* 29:1063–1071.
22. Hauptmann S, *et al.* (2009) Mitochondrial dysfunction: An early event in Alzheimer pathology accumulates with age in AD transgenic mice. *Neurobiol Aging* 30:1574–1586.
23. Moreira PI, Santos MS, Oliveira CR (2007) Alzheimer's disease: A lesson from mitochondrial dysfunction. *Antioxid Redox Signal* 9:1621–1630.
24. Berchtold NC, *et al.* (2008) Gene expression changes in the course of normal brain aging are sexually dimorphic. *Proc Natl Acad Sci USA* 105:15605–15610.
25. Keil U, *et al.* (2004) Amyloid beta-induced changes in nitric oxide production and mitochondrial activity lead to apoptosis. *J Biol Chem* 279:50310–50320.
26. Tocilescu MA, Fendel U, Zwicker K, Kerscher S, Brandt U (2007) Exploring the ubiquinone binding cavity of respiratory complex I. *J Biol Chem* 282:29514–29520.
27. Zhang W, *et al.* (2008) V-ATPase V0 sector subunit a1 in neurons is a target of calmodulin. *J Biol Chem* 283:294–300.
28. Mandelkow EM, Stamer K, Vogel R, Thies E, Mandelkow E (2003) Clogging of axons by tau, inhibition of axonal traffic and starvation of synapses. *Neurobiol Aging* 24:1079–1085.
29. Ittner LM, *et al.* (2008) Parkinsonism and impaired axonal transport in a mouse model of frontotemporal dementia. *Proc Natl Acad Sci USA* 105:15997–16002.
30. Guo JP, Arai T, Miklossy J, McGeer PL (2006) Abeta and tau form soluble complexes that may promote self aggregation of both into the insoluble forms observed in Alzheimer's disease. *Proc Natl Acad Sci USA* 103:1953–1958.
31. Smith MA, Siedlak SL, Richey PL, Mulvihill P, Ghiso J (1995) Tau protein directly interacts with the amyloid beta-protein precursor: Implications for Alzheimer's disease. *Nat Med* 1:365–369.
32. Hansson Petersen CA, *et al.* (2008) The amyloid beta-peptide is imported into mitochondria via the TOM import machinery and localized to mitochondrial cristae. *Proc Natl Acad Sci USA* 105:13145–13150.
33. Mosconi L, *et al.* (2007) Maternal family history of Alzheimer's disease predisposes to reduced brain glucose metabolism. *Proc Natl Acad Sci USA* 104:19067–19072.
34. Oddo S, *et al.* (2003) Triple-transgenic model of Alzheimer's disease with plaques and tangles: Intracellular Abeta and synaptic dysfunction. *Neuron* 39(3):409–421.